Mod Pathol 37 (2024) 100561

MODERN PATHOLOGY

USCAP UNITED STATES AND CANADIAN ACADEMY OF PATHOLOGY
Creating a Better Pathologist

Journal homepage: https://modernpathology.org/

Research Article

Comparison of Primary and Metastatic Fumarate Hydratase-Deficient Renal Cell Carcinomas Documents Morphologic Divergence and Potential Diagnostic Pitfall With Peritoneal Mesothelioma

Anna Caliò[a], Stefano Marletta[a,b], Lavinia Stefanizzi[c], Lisa Marcolini[c], Matteo Rotellini[d], Gabriella Serio[e], Elena Bariani[f], Caterina Vicentini[c], Serena Pedron[a], Filippo M. Martelli[c], Pietro Antonini[a], Matteo Brunelli[a], Guido Martignoni[a,c,*]

[a] *Section of Pathology, Department of Diagnostic and Public Health, University of Verona, Verona, Italy;* [b] *Division of Pathology, Humanitas Istituto Clinico Catanese, Catania, Italy;* [c] *Department of Pathology and Laboratory Medicine, Pederzoli Hospital, Peschiera, Verona, Italy;* [d] *Anatomia Patologica Massa Carrara Azienda Toscana Nord Ovest, Italy;* [e] *Pathology Unit, Department of Precision and Regenerative Medicine and Ionian Area, University of Bari, Italy;* [f] *Unit of Anatomic Pathology, Department of Oncology, Bellaria Hospital, Bologna, Italy*

ARTICLE INFO

Article history:
Received 23 February 2024
Revised 5 June 2024
Accepted 1 July 2024
Available online 10 July 2024

Keywords:
cancer biomarkers
diagnostic pitfall
differential diagnosis
fumarate hydratase
intratumoral heterogeneity
renal cell carcinoma

ABSTRACT

Fumarate hydratase (FH)-deficient renal cell carcinomas are rare neoplasms characterized by wide morphologic heterogeneity and pathogenetic mutations in the *FH* gene. They often show aggressive behavior with rapid diffusion to distant organs, so novel therapeutic scenarios have been explored, including EGFR inhibitors and PD-L1 expression for targeted immunotherapy. Herein, we investigated a series of 11 primary FH-deficient renal cell carcinomas and 7 distant metastases to evaluate tumor heterogeneity even in metastatic sites and estimate the specific spread rates to various organs. Furthermore, the tumors were tested for immunohistochemical PD-L1 expression and *EGFR* mutations. Most metastatic cases involved the abdominal lymph nodes (4/7; 57%), followed by the peritoneum (3/7; 42%), the liver (2/7; 29%), and the lungs (1/7; 14%). Six metastatic localizations were histologically documented, revealing a morphologic heterogeneous architecture often differing from that of the corresponding primary renal tumor. Peritoneal involvement morphologically resembled a benign reactive mesothelial process or primary peritoneal mesothelioma, thus advocating to perform an accurate immunohistochemical panel, including PAX8 and FH, to reach a proper diagnosis. A pure low-grade succinate dehydrogenase–looking primary FH-deficient renal cell carcinoma was also recorded. As for therapy, significant PD-L1 labeling was found in 60% of primary renal tumors, whereas none of them carried pathogenetic *EGFR* mutations. Our data show that FH-deficient renal cell carcinoma may be morphologically heterogeneous in metastases as well, which involve the lymph nodes, the liver, and the peritoneum more frequently than other renal tumors. Due to the high frequency of this latter (42%), pathologists should always be concerned about ruling out mesothelial-derived mimickers, and the occurrence of rarer, primary, low-grade–looking types. Finally, contrary to *EGFR* mutations, PD-L1 expression could be a possible predictive biomarker for the therapy of these tumors.

These authors contributed equally to this work: Anna Caliò and Stefano Marletta.

* Corresponding author.
E-mail address: guido.martignoni@univr.it (G. Martignoni).

https://doi.org/10.1016/j.modpat.2024.100561

Introduction

Fumarate hydratase (FH)-deficient renal cell carcinoma is a rare renal neoplasm pathogenetically characterized by germline or somatic biallelic inactivation of the *FH* gene, currently included among the "molecularly defined renal cell carcinomas" category by the World Health Organization (WHO) classification.[1,2] First described as a familiar disease, often associated with cutaneous and uterine leiomyomas in the so-called "hereditary leiomyomatosis and renal cell carcinoma syndrome,"[3] it has been recently shown that about 20% of these tumors occur in a sporadic setting.[4] Microscopically, they were initially described as tumors growing in papillary structures composed of cells with voluminous eosinophilic cytoplasm, usually with prominent eosinophilic nucleoli.[5] Over the years, several architectural patterns have been accustomed to these neoplasms, including solid, tubule-cystic, cribriform, sieve-like, and nested, among others.[5-8] This expanding morphologic spectrum of the primary renal tumor resulted in challenging differential diagnosis. Along with the high-grade nuclear features, an aggressive clinical course has been reported, with metastatic spread to lymph nodes and many distant organs.[3,9] However, no data on the histopathologic features of the distant metastases have been reported so far. The knowledge of morphologic findings of the metastatic sites is of paramount importance as, in recent years, bioptic samples of distant metastases have often been obtained to reach proper diagnosis and offer therapy.

Concerning therapy, no specific drug has been approved for FH-deficient renal cell carcinoma.[10] Therefore, patients are generally administered treatment usually employed for more common renal carcinomas, even though immune checkpoint inhibitor (ICI) monotherapies seem to control the disease better.[4] In this setting, increased PD-1/PD-L1 expression has been reported in a restricted proportion of these tumors, potentially identifying a subset of patients who may benefit from ICIs.[11,12] In addition, patients diagnosed with advanced diseases have been variably given combined EGFR/VEGF inhibitor regimens without any predictive biomarker.[13,14]

In this study, we describe 11 cases of FH-deficient renal cell carcinomas, highlighting the microscopic characteristics of the distant metastases with particular interest in peritoneal involvement and its diagnostic pitfall. Moreover, PD-1/PD-L1 expression, the composition of different lymphocyte subpopulations, and the eventual presence of *EGFR* gene mutations have been investigated.

Materials and Methods

Patients and Samples

Eleven cases of FH-deficient renal cell carcinomas, one previously described,[15] were retrieved from the files of participant institutions, including samples from both primary neoplasms and distant metastases when available. Five were in-house patients, whereas 6 were consultation cases. All procedures performed in our study involving human participants received approval (Prog. 4136CESC) and were in accordance with the ethical standards of the institutional and/or national research committee and with the declaration of Helsinki. Clinical data on a previous history of other renal tumors in relatives and of personal extrarenal neoplasm were also recorded. All slides were reviewed by 3 authors (A.C., S.M., and G.M.). For each case, the following pathologic features were assessed: the architectural growth pattern, the nucleolar grade according to the International Society of Urological Pathology (ISUP)/WHO, the presence of coagulative granular necrosis, the pTNM stage according to the 8th edition of the American Joint Committee on Cancer Staging Manual, and the presence/absence of tumor-infiltrating lymphocytes (TILs). The distribution of immune infiltrates, when present, was graded into 3 categories as suggested by previous studies[16,17]: "desert" (no TILs either within the tumor or its periphery), "excluded" (TILs just accumulate around the tumor without relevant permeation within the lesion), and "inflamed" (TILs are intermixed with the neoplastic cells in the whole tumor area). Follow-up data regarding the development of distant metastases and/or local recurrence were collected from electronic health databases relying on the available pathologic and radiological records.

Immunohistochemistry

Sections from tissue blocks of the retrieved tumors were immunohistochemically (IHC) stained for PAX8 (clone MRQ-50, prediluted; Roche), CK8-18 (clone 5D3, dilution 1:100; Leica), CK7 (clone RN7, dilution 1:100; Novocastra), WT1 (clone WT49, dilution 1:20; Leica), AMACR (clone 13H7, dilution 1:25; Dako), S100A1 (clone M01, dilution 1:600; Abnova), calretinin (clone 566, dilution 1:200; Leica), Ber-EP4 (clone Ber-EP4, dilution 1:100; Abcam), cathepsin K (clone 3F9, dilution 1:1600; Abcam), INI1 (clone 25/BAF47, prediluted; Master Diagnostica), succinate dehydrogenase (SDH)B (clone 21A11AE7, dilution 1:800; Abcam), FH (clone J-13 , dilution 1:50; Santa Cruz Biotech), and PD-1 (clone CAL-20, prediluted; Roche). Moreover, tumors defined as "excluded" and "inflamed" based on hematoxylin and eosin staining were investigated for the specific composition of different lymphocyte subpopulations according to the different percentages of expression of the following antibodies: CD3 (clone PS1, dilution 1:200; Leica), CD20 (clone L26, prediluted, Novocastra), CD4 (clone 4B12, dilution 1:150; Leica), CD8 (clone 29S, dilution 1:20; Leica), and GATA3 (clone L50-823, dilution 1:150; BD Pharmingen). In all the pseudomesothelial peritoneal deposits, BAP1 (clone C4, dilution 1:250; Santa Cruz Biotech) was carried out. All samples were processed using a sensitive "Bond Polymer Refine" detection system in an automated Bond IHC instrument (Leica Biosystems). The most commonly used IHC assay developed to determine PD-L1 expression level was performed (clone SP263, prediluted; Roche) on the Ventana Benchmark Ultra platform (Ventana) according to the manufacturer's instructions. Membranous immune expression of PD-L1 on neoplastic cells was recorded as the percentage of positive neoplastic elements. The appropriate positive (tonsil and placenta) and negative controls were concurrently performed. As controls for PAX8 and S100A1, 10 pleural mesotheliomas, 3 peritoneal mesotheliomas, and 20 omental mesothelial hyperplasia were carried out.

EGFR Molecular Analysis

DNA was extracted from consecutive 4-μm-thick formalin-fixed, paraffin-embedded sections from both primary tumors and metastases when available (cases 1, 2, and 7) with a percentage of tumoral cells ranging from 30% to 80% through a QIAamp DNA formalin-fixed, paraffin-embedded kit (Qiagen) and then quantified using Nanodrop Spectrophotometer (ThermoFisher Scientific). Mutational *EGFR* gene status was investigated using the EasyPGX-ready EGFR kit (Diatech Pharmacogenetics). It is a complete qualitative real-time PCR in vitro diagnostic solution able to detect the main mutations of exons 18, 19, 20, and 21 of the

EGFR gene using 8 oligo mixes. Each mix allows the coamplification of one or more mutated alleles plus an endogenous control gene. A specific control mix enables the evaluation of the DNA quality and quantity of each sample.

Statistical Analysis

Fisher exact test was used to compare the distribution of TILs and PD-L1 staining, distinguishing between significant and nonsignificant levels according to the median value of the expression. *P* values were based on a 2-tailed hypothesis. The results were considered statistically relevant if the *P* value was less than .05.

Results

Clinical and Pathologic Features

The clinical and pathologic features of the 11 patients are detailed in Table 1. Four patients were women, and 7 were men (F:M ratio, 1:1.75). An underlying hereditary syndrome was confirmed in 3 cases, including 2 siblings (patients 7 and 8) and a woman with a previous history of uterine leiomyomas and skin papules (patient 11). Therefore, in such instances, a "hereditary leiomyomatosis and renal cell carcinoma syndrome" condition was established. Age at diagnosis ranged from 33 to 66 years (mean, 51; median, 48). Primary renal tumors were removed using radical nephrectomy in majority of the cases (9/11; 82%), whereas 2 patients (cases 1 and 9) underwent nephron-sparing surgery. The tumors ranged in size from 5 cm to 9 cm (mean, 6.5; median, 7.3) **(**Fig. 1**)**. Morphologically, various and often intermingled architectural growth patterns were observed, ranging from papillary to tubule-cystic, the predominant pattern, followed by tubule-glandular, alveolar, and solid, as shown in Table 1. Foci of coagulative granular necrosis were identified in 3 cases (27%; cases 8, 10, and 11). Concerning nucleolar grade, according to the ISUP/WHO classification, 9 tumors were classified as high-grade (G3-G4), namely 6 G3 and 3 G4 displaying sarcomatoid dedifferentiation (27%; cases 8, 10, and 11) **(**Fig. 2**)**. One tumor (case 4) was entirely low-grade G2 and another one (case 5) was characterized by low-grade foci associated with separate high-grade (G3) areas, as previously described.[15] TILs were respectively scored as "desert" in 63% (7/11), "excluded" in 27% (3/11), or "inflamed" in 10% (1/11) of the samples.

Follow-up was available for 10 patients, ranging from 10 to 77 months (mean, 35; median, 26). Eight cases displayed aggressive clinical behavior, which was as follows: 1 case developed local recurrence, 6 cases developed distant metastases, and another 1 developed both local recurrence and distant metastases (case 1). Four distant metastases were histologically documented (patients 1, 2, 3, and 7). The site of metastatic disease was variable, including abdominal lymph nodes (4 cases, 2 of them histologically documented, both with the tubule-glandular architecture), the liver (2 cases, 1 histologically confirmed with the tubule-glandular architecture), the lungs (1 case), and the peritoneum (3 cases, all histologically documented). Architectural patterns of primary renal tumors and corresponding metastases are compared in Table 2 and displayed in Figure 3. The peritoneal localizations are separately described in the following sections owing to their peculiar morphologic features, diagnostic pathologic pitfall, and clinical implications, and summarized in Table 3. Moreover, because of their rarity, a separate paragraph has been included to report 2 cases of low-grade oncocytic FH-deficient renal cell carcinoma.

Peritoneal-Spreading Tumors With a "Pseudomesotheliomatous" Appearance

Case 1

A 46-year-old male patient underwent partial nephrectomy for a 6.5-cm left renal tumor. The tumor was microscopically arranged in a tubule-cystic architecture with a minor component of high-grade carcinomatous-looking tubule-glandular structures, focally invading the perirenal adipose tissue. At that time, the initial diagnosis was tubule-cystic renal cell carcinoma with poorly differentiated foci.[18] Three years after the surgery, a left-sided peritoneal mass was detected with a magnetic resonance imaging scan and then removed. During the surgical procedure, the urologist faced an unusual gross finding resembling the peritoneal inclusion cysts. The frozen section interpretation was extremely challenging, showing lobules of adipose tissue lining by a tubule-cystic proliferation of cuboidal cells characterized by round nuclei with prominent eosinophilic nucleoli resembling mesothelial cells. The IHC analysis revealed positive immune staining of the tubule-cystic proliferation for PAX8, AMACR, S100A1, Ber-EP4, and BAP1 along with negativity for CK7, WT1, and calretinin, supported the diagnosis of a peritoneal localization of the primary renal tumor. The revision of the primary tumors and the peritoneal localization demonstrated the loss of FH in both neoplasms.

Case 2

A computed tomography scan in a 66-year-old female patient revealed multiple nodal, lung, and peritoneal nodules above the liver and the abdominal skeletal muscles, suspicious of metastases. Two years before, she had been diagnosed with a papillary renal cell carcinoma, G3, removed using radical nephrectomy. To reach a histologic diagnosis, a peritoneal nodule was biopsied. Light microscopy showed a proliferation of small papillary structures made up of fibro-vascular cores covered by medium-sized "hobnail"-looking eosinophilic epithelioid cells, with roundish, luminally oriented nuclei and often prominent nucleoli (Fig. 4**A**). Relying on these morphologic features, a differential diagnosis between a mesothelial process and a localization of serous carcinoma was made. The IHC expression of PAX8 (Fig. 4**B**), AMACR, S100A1, Ber-EP4 (Fig. 4C), and BAP1 by neoplastic cells supported a peritoneal metastasis by a renal cell neoplasm, further strengthened by their negativity for mesothelial markers. Moreover, the IHC loss of the FH staining (Fig. 4D) suggested the hypothesis of peritoneal metastasis of FH-deficient renal cell carcinoma. A histologic review of the slides of the primary kidney tumor, supported by an additional IHC analysis, confirmed such a diagnosis for the removed renal mass as well.

Case 3

Following an ultrasound examination with unspecific findings performed for abdominal pain, a 48-year-old man was discovered with a 20-cm left pelvic-hypochondria lesion on a computed tomography scan. Thus, the patient underwent laparoscopic resection of the mass. Histologically, it was composed of solid and tubule-cystic structures recalling mesothelial proliferation. Hence, it was initially diagnosed as multicystic benign mesothelioma. One year later, multiple peritoneal nodules were detected on magnetic resonance imaging, as well as a 6.7-cm mass close to the left kidney. Both the peritoneal nodules and the perirenal mass

Table 1
Clinical and pathologic features of fumarate hydratase-deficient renal cell carcinomas of the present series

Case no.	Sex	Age (y)	Size (cm)	Laterality	Surgery	Gross	Invasion	pTNM	ISUP/WHO grade	Necrosis	Follow-up (mo)	Metastasis	Leiomyomas	Sporadic/ hereditary	NNo. of slides with tumor	Histologic pattern
1	M	46	6.5	L	PN	Single	Perinephric fat	pT3aNxM1	3	Absent	77 (AWD)	Local recurrence and peritoneum	NA	NA	36	99% Tubule-cystic and 1% tubule-glandular
2	F	66	4.3	R	RN	Single	Renal sinus fat	pT3aN1M1	3	Absent	14 (AWD)	Lymph nodes, peritoneum, and lung	NA	Sporadic	2	99% Papillary and 1% tubule-glandular
3	M	48	6.7	L	RN	Single	Perinephric fat	pT3aN0M1	3	Absent	20 (AWD)	Peritoneum	NA	NA	1	100% Tubule-cystic
4	M	48	7	R	RN	Single	Absent	pT1bNxMx	2	Absent	36 (NED)	NA	NA	NA	37	100% Alveolar
5[a]	M	41	5	L	RN	Single	Renal sinus fat	pT3aNxMx	3	Absent	53 (AWD)	Local recurrence	NA	NA	53	80%-90% Tubule-cystic and 10%-20% solid
6	F	58	8	L	RN	Single	Absent	pT2N2M1	3	Absent	26 (AWD)	Lymph nodes and liver	Uterus	NA	2	80% Tubule-glandular, 15% solid, and 5% tubule-cystic
7[b]	M	62	5	L	RN	Single	Perinephric and renal sinus fat	pT3bN1M1	3	Absent	DOD	Lymph nodes and liver	NA	Hereditary	17	55% Tubule-cystic, 40% sieve-like, and 5% papillary
8[b,c]	M	49	6	R	RN	Single	Perinephric and renal sinus fat	pT3aNxMx	4	Present	42 (DOD)	Liver	NA	Hereditary	12	40% Papillary, 40% solid, 15% tubule-glandular, and 5% sarcomatoid
9	F	44	NA	R	PN	Single	NA	pTxN1Mx	3	Absent	AWD	Lymph nodes	Uterus	NA	1	90% Tubule-cystic and 10% papillary
10[c]	M	33	9	L	RN	Single	Absent	pT2NxMx	4	Present	NA	NA	NA	NA	1	90% Sarcomatoid and 10% papillary
11[c]	F	62	5.5	L	RN	Single	Perinephric and renal sinus fat	pT3aNxMx	4	Present	10 (NED)	NA	Uterus and skin	Hereditary	30	60% Solid and 40% sarcomatoid

AWD, alive with disease; DOD, dead of disease; ISUP/WHO, International Society of Urological Pathology/World Health Organizaion; NA, not available; NED, no evidence of disease; PN, partial nephrectomy; RN, radical nephrectomy.

[a] Previously described by Smith et al.[15]

[b] Siblings.

[c] Sarcomatoid dedifferentiation.

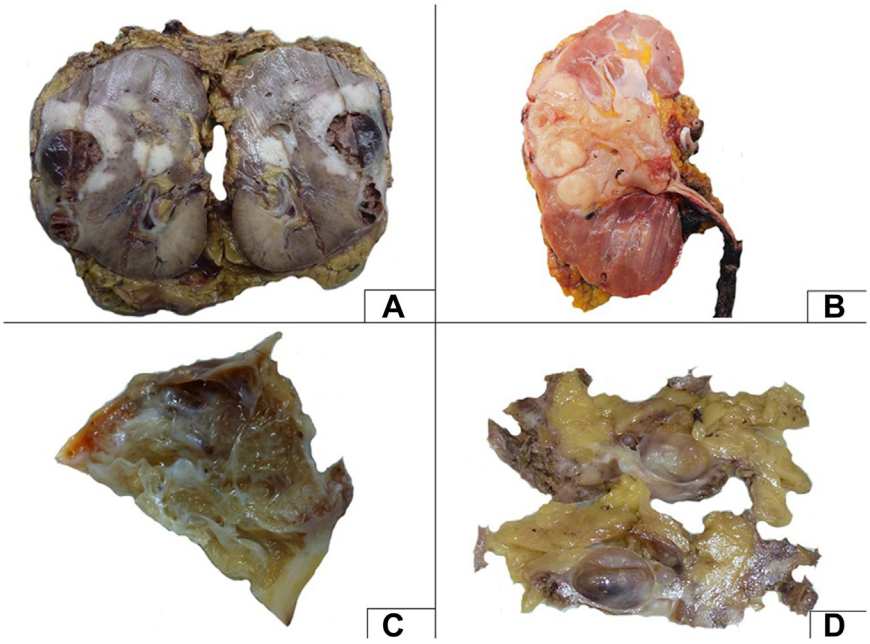

Figure 1.
Gross features of fumarate hydratase-deficient renal cell carcinoma. (A) Radical nephrectomy from case 8 showing a whitish solid tumor with ill-defined borders and a large hemorrhagic area. (B) Radical nephrectomy from case 11 revealing a solid grayish neoplasm with a nodular appearance and pushing margins. (C) Nephron-sparing surgery from case 5 displaying a multicystic-appearing lesion. (D) Surgical resection of peritoneal localization from case 1 showing multicystic-looking areas mixed with whitish, ill-defined solid areas infiltrating the surrounding adipose tissue.

were then surgically resected. Pathologic examination showed a solid and tubule-cystic proliferation, reminiscing of the previously removed one made up of clear to eosinophilic cells often displaying prominent nucleoli (Fig. 4E). Immunohistochemically, the neoplastic cells stained positive for PAX8 (Fig. 4F), AMACR, Ber-EP4 (Fig. 4G), S100A1, and BAP1 while labeling negative for CK7, WT1, and calretinin. In addition, no expression of the FH was observed (Fig. 4H). Thus, a diagnosis of FH-deficient renal cell carcinoma with secondary peritoneal localizations was rendered. Finally, 2 months later, left radical nephrectomy with lymphadenectomy was performed. Light microscopy revealed scattered residual foci of a neoplasm partially involving the perirenal fat, harboring overlapping morphologic features and immunophenotype with the previously removed specimens. An associated granulomatous inflammatory reaction related to the former surgical procedure was also noticed.

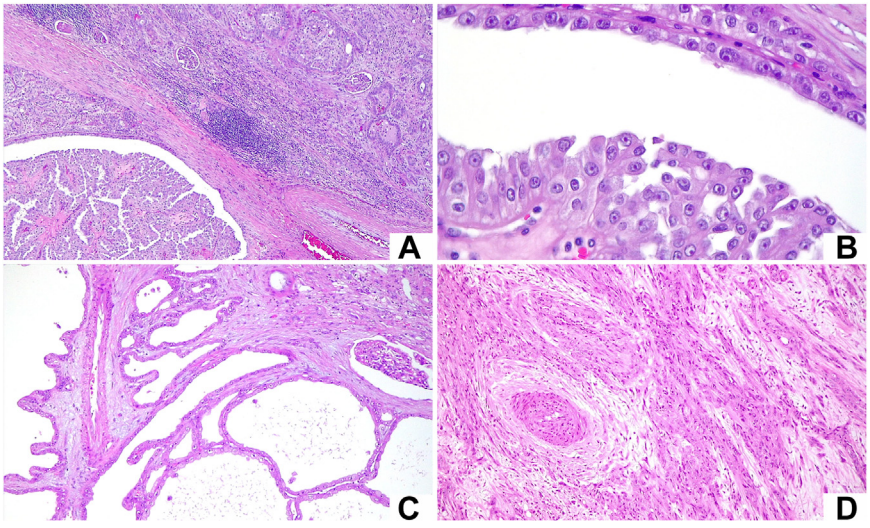

Figure 2.
The morphologic pattern of fumarate hydratase-deficient renal cell carcinoma. (A) A low-power picture from case 2 revealing a predominantly papillary-arranged neoplasm. (B) Higher magnification of the previous case highlighting high-grade cytologic features such as prominent eosinophilic nucleoli. (C) A primary renal tumor of case 7 prevalently arranged in a tubule-cystic architecture. (D) Microphotographs of case 8 showing sarcomatoid-looking foci.

Table 2
Architectural composition of renal tumor and histologically documented metastatic localizations of fumarate hydratase-deficient renal cell carcinomas of the present series

Histologic pattern	Tubule-cystic	Tubule-glandular	Papillary	Solid	Alveolar	Sieve-like	Sarcomatoid
Case no.							
1[a]	99%	1%					
1[b] (peritoneum)	99%	1%					
2[a]		1%	99%				
2[b] (peritoneum)			100%				
2[b] (lymph node)		100%					
3[b] (peritoneum)	98%			2%			
4[a]					100%		
5[a]	80%				20%		
5[a] (local recurrence)	90%				10%		
6[a]	5%	80%		15%			
7[a]	55%		5%			40%	
7[b] (lymph node)		100%					
7[b] (liver)		100%					
8[a]		15%	40%	40%			5%
9[a]	90%		10%				
10[a]			10%				90%
11[a]				60%			40%

[a] Renal tumor.
[b] Metastasis.

Low-Grade Oncocytic Tumors Resembling Succinate Dehydrogenase–Deficient Renal Cell Carcinoma

Case 4

A 48-year-old male patient underwent radical nephrectomy for a 7-cm right renal mass. Grossly, the tumor was located in the central zone of the kidney and was brownish in color at the cut examination. Microscopically, the lesion was composed of roundish eosinophilic cells displaying a solid-nested to tubule-alveolar growth pattern (Fig. 5A). Neoplastic cells revealed low-grade microscopic hallmarks, showing barely inconspicuous nucleoli (G2 ISUP/WHO grading) and no evidence of coagulative granular necrosis or significant mitotic activity (Fig. 5B). The tumor was wholly embedded, showing a homogeneous morphologic pattern within the entire neoplasm. The histologic features were consistent with a low-grade oncocytic renal tumor, reminiscing an SDH-deficient renal cell carcinoma at first glance, further suggested by its negativity for CK8-18. Nevertheless, IHC assays detected retained expression of SDH (Fig. 5C), ruling out such a diagnosis. Conversely, neoplastic cells failed to stain for FH (Fig. 5D), leading to the definitive diagnosis of low-grade oncocytic FH-deficient renal cell carcinoma. To date, after 36 months, the patient is alive with no evidence of local recurrence or distant metastases.

Case 5

As previously reported,[15] a 41-year-old male patient underwent partial resection with nephron-sparing surgery of an incidentally discovered 5-cm left renal mass. Microscopically, the lesion was made up of low-grade polygonal eosinophilic cells displaying a multicystic to solid-nested growth pattern. In these latter foci, the neoplastic cells showed flocculent cytoplasm, sometimes with vacuoles containing eosinophilic inclusion-like

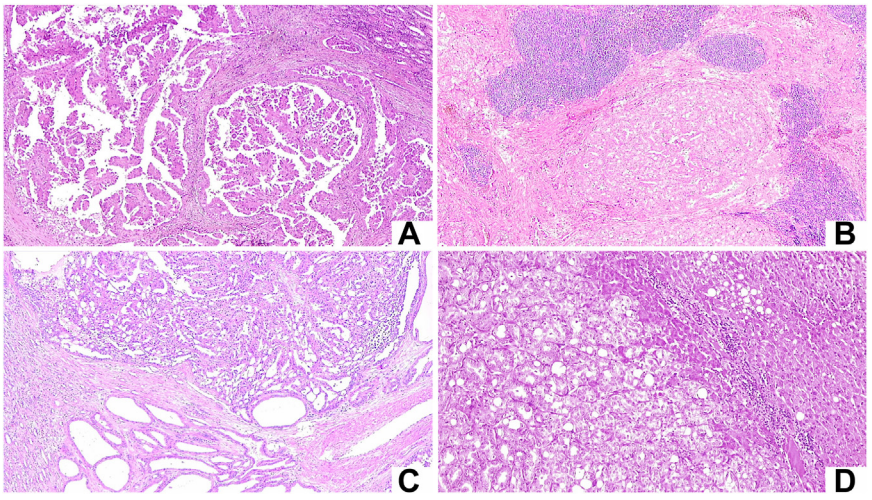

Figure 3.
Comparison of the architectural pattern between primary tumors and metastases. (A) A primary renal tumor growing with a papillary architecture, compared with (B) tubule-glandular structures of the corresponding lymph node metastasis. (C) Tubule-cystic and sieve-like arrangement of the kidney neoplasm of case 7, opposite to (D) a tubule-glandular pattern in the liver metastasis.

Table 3
Pathologic and immunohistochemical findings of tumors metastatic to the peritoneum

Case no.	Previous history of RCC	Histologic pattern	CK8-18	PAX8	CK7	WT1	AMACR	CALR	Ber-EP4	BAP1	FH
1	Yes	Tubule-cystic and tubule-glandular	+	+	Neg.	Neg.	+	Neg.	+	Retained	Loss
2	Yes	Papillary	+	+	Neg.	Neg.	+	Neg.	+	Retained	Loss
3	No	Solid and tubule-cystic	+	+	Neg.	Neg.	+	Neg.	+	Retained	Loss

AMACR, alpha-methylacyl-CoA racemase; CALR, calretinin; CK, cytokeratin; FH, fumarate hydratase; Neg., negative; RCC, renal cell carcinoma.

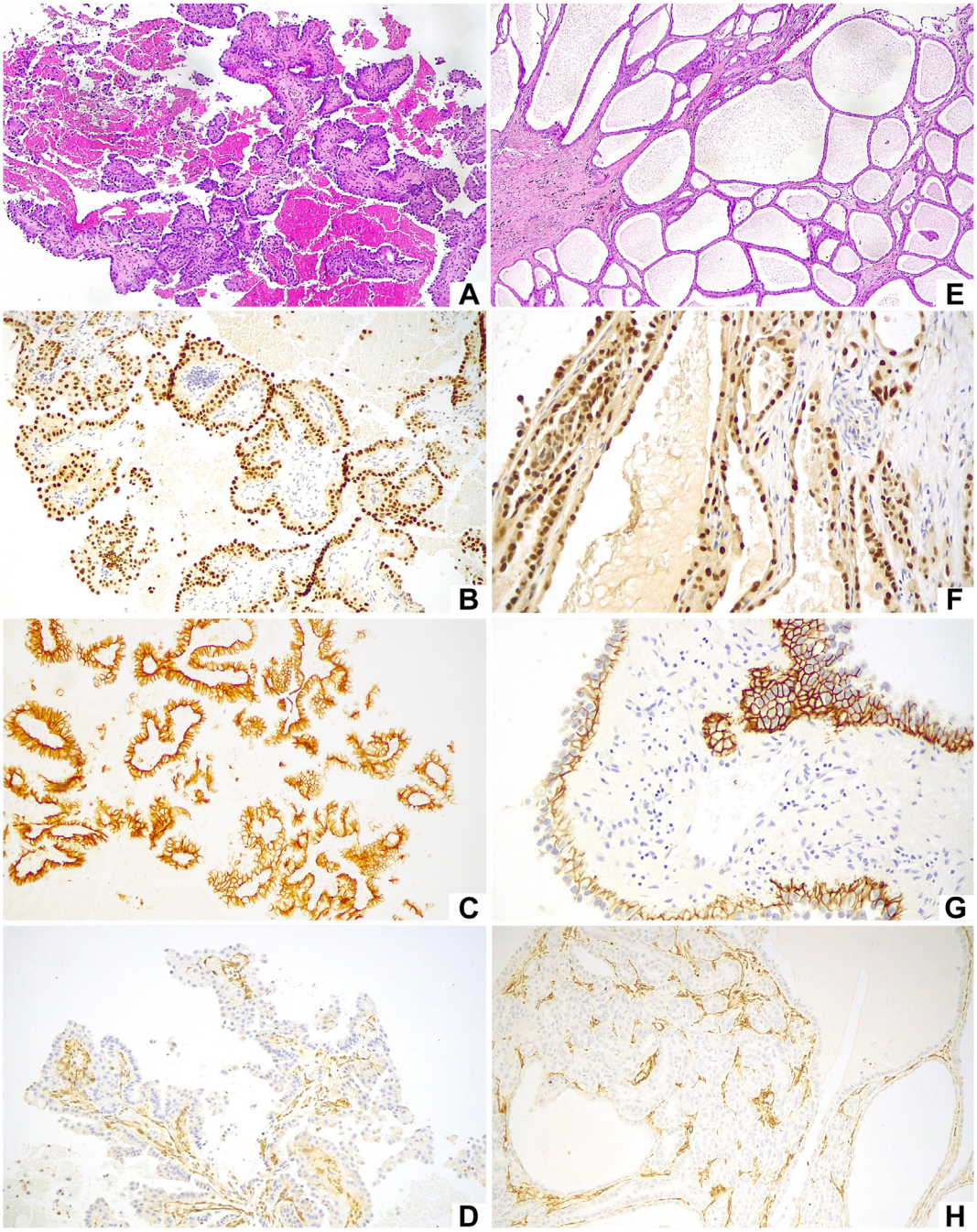

Figure 4.
The pseudomesotheliomatous pattern of fumarate hydratase (FH)-deficient renal cell carcinoma. (A) Peritoneal localization from case 2, represented by a papillary proliferation of eosinophilic cells, closely resembling mesothelial hyperplasia. The neoplastic cells labeled positive for (B) PAX8 and (C) Ber-EP4, while revealing (D) the loss of FH immunohistochemical expression. (E) Peritoneal metastasis from case 3, made up of eosinophilic cells arranged in a tubule-cystic architecture recalling a multicystic mesothelioma. Immunohistochemical analysis revealing positive staining for (F) PAX8 and (G) Ber-EP4, along with (H) negativity for FH.

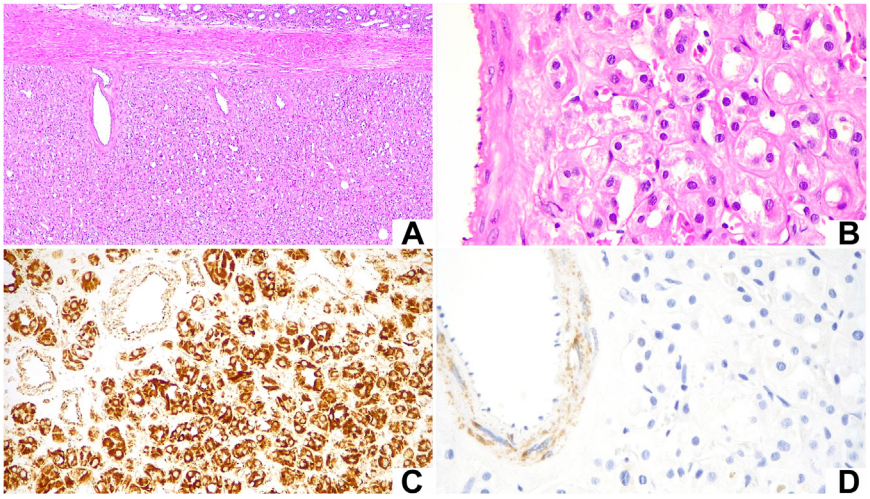

Figure 5.
Low-grade oncocytic fumarate hydratase-deficient renal cell carcinoma. (A) A low-power picture from case 4, homogenously composed of eosinophilic roundish cells with a solid-alveolar growth pattern. (B) At higher magnification, the tumor cells displayed bland-looking hallmarks, similar to barely inconspicuous nucleoli and no relevant mitotic activity, thus mimicking succinate dehydrogenase–deficient renal cell carcinoma. However, immunohistochemical assays revealed (C) retained succinate dehydrogenase staining along with (D) a loss of fumarate hydratase expression.

bodies. So, the morphologic picture was consistent for a low-grade eosinophilic renal tumor, suggesting an SDH-deficient renal cell carcinoma. However, IHC analysis revealed retained SDH expression, along with a loss of FH IHC labeling, supporting the diagnosis of a low-grade oncocytic FH-deficient renal cell carcinoma. Although the pathologic diagnosis advocated for completion nephrectomy, it was only performed 4 years later. The whole removed kidney showed a high-grade (G3-G4) renal cell carcinoma with tubule-glandular, solid, and tubule-cystic architecture infiltrating the renal sinus adipose tissue. The neoplastic cells revealed variably shaped nuclei with perinuclear halos and prominent inclusion-like nucleoli. Thus, compared with the previously excised neoplasm, the cytologic appearance of the novel tumor was much more reminiscent of classic FH-deficient renal cell carcinomas, further confirmed based on IHC assays. Finally, 3 months after the completion of the radical nephrectomy, a 2.3-cm nodule in the left renal fossa suspicious of local recurrence was detected at imaging examination and then surgically removed. Pathologic examination confirmed the radiological suspicion, showing a high-grade neoplasm with overlapping morphologic and IHC features with the former one.

Immunohistochemistry and Tumor Microenvironment Findings

The IHC results are tabulated in Table 4. All the tumors stained positive for PAX8 and the proximal tubular marker S100A1 (11/11; 100%), with a percentage of positive cells that ranged from 10% to 100%, while labeling negative for cathepsin K. Similarly, apart from 1 sample (case 4), CK8-18 was widely expressed by the tumors of the entire series (10/11; 91%). In contrast, all but one neoplasm (10/11; 91%) were, respectively, negative for CK7 (case 2) and for the distal tubular marker GATA3 (case 4). With regard to other IHC markers commonly used in routine practice, staining for AMACR was variably detected in most of the samples tested (7/11; 64%), ranging from 10% to 90% of neoplastic cells. Expression of SDHB and INI1 was retained in all the cases (11/11; 100%), along with a loss of FH IHC staining. None of the pleural and peritoneal mesothelioma or omental mesothelial hyperplasia expressed PAX8 or S100A1.

As for the specific composition of TILs, generally, both "excluded" and "inflamed" samples showed a prevalent CD3+ T-lymphocyte response, variably making up from 50% to 90% of overall immune cells (Fig. 6A). Namely, a CD8+ T-cytotoxic

Table 4
Immunohistochemical findings and characteristics of tumoral microenvironment of fumarate hydratase-deficient renal cell carcinomas of the present series

Case no.	PAX8	CK8-18	CK7	AMACR	S100A1	GATA3	SDH	FH	CATK	INI1	TILs	PD-L1	PD-1	CD3	CD20	CD4	CD8
1	90% +	80% +	Neg.	90% +	80% +	Neg.	+	Neg.	Neg.	+	Desert	Neg.	Neg.				
2	40% +	90% +	90% +	90% +	40% +	Neg.	+	Neg.	Neg.	+	Excluded	10% +	Neg.	10%	90%	10%	90%
3	90% +	90% +	Neg.	90% +	50% +	Neg.	+	Neg.	Neg.	+	Desert	NA	NA				
4	90% +	Neg.	Neg.	Neg.	70% +	90% +	+	Neg.	Neg.	+	Desert	10% +	Neg.				
5[a]	90% +	80% +	Neg.	70% +	90% +	Neg.	+	Neg.	Neg.	+	Desert	Neg.	Neg.				
6	100% +	100% +	Neg.	90% +	80% +	Neg.	+	Neg.	Neg.	+	Desert	5% +	<1%				
7[b]	90% +	100% +	Neg.	10% +	20% +	Neg.	+	Neg.	Neg.	+	Excluded	2% +	<1%	50%	50%	10%	90%
8[b]	30% +	90% +	Neg.	10% +	10% +	Neg.	+	Neg.	Neg.	+	Desert	30% +	<1%				
9	100% +	50% +	Neg.	Neg.	30% +	Neg.	+	Neg.	Neg.	+	Excluded	10% +	Neg.	50%	50%	10%	90%
10	60% +	70% +	Neg.	Neg.	90% +	Neg.	+	Neg.	Neg.	+	Desert	5% +	Neg.				
11	70% +	40% +	Neg.	Neg.	10% +	Neg.	+	Neg.	Neg.	+	Inflamed	70% +	Neg.	90%	10%	10%	90%

AMACR, alpha-methylacyl-CoA racemase; CATK, cathepsin K; CK, cytokeratin; FH, fumarate hydratase; NA, not available; Neg., negative; SDH, succinate dehydrogenase; TILs, tumor-infiltrating lymphocytes.
[a] Previously described by Smith et al.[15]
[b] Siblings.

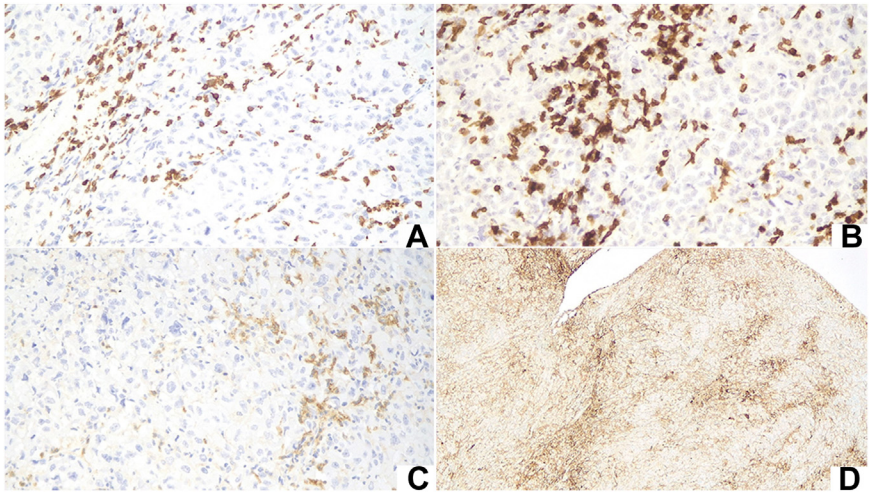

Figure 6.
Tumor-infiltrating lymphocytes and PD-L1. (A) "Inflamed" tumor microenvironment (case 11), with a conspicuous amount of CD3+ T lymphocytes intermixed with the neoplastic cells, mainly made up of (B) CD8+ T-cytotoxic lymphocytes and (C) a minor percentage of CD4+ T-helper lymphocytes. (D) The same case revealing strong and diffuse PD-L1 immunohistochemical expression in the great majority (70%) of neoplastic cells.

response was significantly prevalent in both tumors effaced by a peripheral ("excluded") and a remarkable ("inflamed") inflammatory infiltrate (Fig. 6B, C). Overall, CD20+ B lymphocytes accounted for a restricted proportion of all the inflammatory cells. A prominent B-lymphocyte–related response was observed in one "excluded" sample (case 2). Only a few scattered GATA3+ Th-2 lymphocytes were detected. As far as potentially druggable markers were concerned, at least focal IHC expression of PD-L1 on neoplastic elements was found in a noteworthy proportion of the tumors tested, ranging from 2% to 70% of the cells (mean, 17%; median, 10%), whereas none of them (nor the adjacent inflammatory infiltrate) significantly stained for PD-1. Interestingly, the 2 cases with a higher percentage of PD-L1 expression were 2 cases with sarcomatoid dedifferentiation (cases 8 and 11). Moreover, the strongest and most diffuse PD-L1 expression was observed in the only "inflamed" tumor (case 11; Fig. 6D). However, no relevant statistical association was, overall, found with the distribution of TILs, neither when considering "desert" plus "excluded" vs "inflamed" tumors ($P = 1.000$) nor when matching "desert" vs "excluded" plus "inflamed" neoplasms ($P = .523$).

EGFR Molecular Analysis

No targeted mutations in exons 18, 19, 20, or 21 of the *EGFR* gene were detected in any tumor samples.

Discussion

Increased data collected in recent years have identified the multiplicity of admixed architectural growth patterns in primary renal tumors as the most common and relevant morphologic features of FH-deficient renal cell carcinomas.[1,6-8] Most of the samples from our series (10/11; 91%) displayed at least 2 different histologic components, spanning from papillary to tubule-cystic, solid, sieve-like, and nested growth patterns. This high histologic variability is similar to that in other reports, observed in about 90% of the cases in some series.[3,6] However, the morphologic features of metastases were never analyzed.[6] In this study, we reported 6 histologically documented FH-deficient renal cell carcinoma metastases from 4 patients from different sites, including lymph nodes, the liver, and the peritoneum, demonstrating different architectural patterns. For this reason, it could be extremely challenging to reach a proper pathologic diagnosis, particularly when the clinical information is limited. In fact, owing to their aforementioned histologic heterogeneity, they may be easily misdiagnosed for carcinomas arising from other organs, especially when peritoneal localizations are discovered. Similar to FH-deficient renal cell carcinoma, mesothelial neoplasms may show highly variable microscopic arrangements, ranging from tubule-cystic to papillary structures and to sarcomatoid-looking neoplastic cells.[19,20] Pathologists are not so unlikely to have to deal with similar instances, as nowadays an initial histologic bioptic approach to suspicious metastatic lesions rather than

Table 5
Distribution of metastatic sites between fumarate hydratase-deficient RCC (literature review[3,5,6,21-24] and present series) and other histotypes of RCC[1,25-29]

Metastatic site	FHdRCC	ccRCC[25]	pRCC[26]	chRCC[26]	*TFE3*-rearranged RCC[27]	*TFEB*-rearranged RCC[28]	*TFEB*-amplified RCC[29]	*ALK*-rearranged RCC[1]
Lymph nodes	59/87, 68%	22%	69%	51%	29%	15%	47%	83%
Bones	23/87, 26%	29%	29%	33%	13%	23%	29%	5%
Liver	18/87, 21%	20%	22%	34%	17%	23%	29%	5%
Lungs	18/87, 21%	45%	49%	36%	25%	38%	47%	17%
Peritoneum	11/87, 13%	<3%	5%	4%	5%	0%	12%	0%
Adrenal glands	11/87, 13%	9%	7%	6%	<2%	8%	24%	11%
Brain	1/87%, 1%	8%	3%	2%	1%	0%	7%	17%

ccRCC, clear cell renal cell carcinoma; chRCC, chromophobe renal cell carcinoma; FHdRCC, fumarate hydratase-deficient renal cell carcinoma; pRCC, papillary renal cell carcinoma; RCC, renal cell carcinoma.

primary tumors is an increasingly more common practice. It is worth mentioning that data from our series underline how, similar to primary renal tumors, secondary localizations from FH-deficient renal cell carcinoma may show a broad histologic spectrum. So, the architectural growth pattern of peritoneal and other distant metastases may not only significantly differ from primary renal tumors but also can be extremely variable within the same metastatic lesion. For instance, 2 of the 3 histologically documented peritoneal metastases (cases 1 and 3) showed 2 morphologic patterns, with tubule-cystic structures admixed with tubule-glandular and solid areas, respectively. On the other hand, in case 7, although the primary renal tumor was composed of variable percentages of tubule-cystic, sieve-like, and papillary foci, its corresponding liver and nodal metastases were entirely arranged in a tubule-glandular architecture, not observed in the kidney. To the best of our knowledge, such intratumoral heterogeneity in FH-deficient renal cell carcinoma peritoneal metastases has not been reported so far and further contributes to the challenging work of addressing the proper pathologic diagnosis. Moreover, the frequency of peritoneal spread in such tumors is in more than a third of metastatic cases (3/7; 42%), a higher value than the rate of previous studies (7%-16%).[5-7,9] Pathologists should be aware of these findings when dealing with peritoneal samples, as FH-deficient renal cell carcinomas may have a striking "pseudomesotheliomatous" appearance, closely resembling mesothelial hyperplasia or even primary peritoneal mesothelioma. In such complex cases, high pathologic suspicion is the key to addressing the following IHC tests and then getting into definitive diagnosis. This consideration is of particular concern when a previous history of renal neoplasm is not on record, similar to the third case described in our series, which was initially diagnosed as multicystic peritoneal mesothelioma. In this scenario, a thoughtful IHC panel is worth to figure the diagnostic quandary out. As far as our cohort was concerned, all peritoneal-involving tumors were negative for mesothelial markers calretinin, WT1, and CK7 while conversely constantly labeling for PAX8. Their potential metastatic nature was further suggested by positive staining for Ber-EP4, BAP1, AMACR, and S100A1 and, of course, finally confirmed by the IHC loss of FH.

Furthermore, we observed a high occurrence of lymph nodes and liver metastases (4/7 [57%] and 2/7 [29%], respectively) rather than the lungs (1/7; 14%). Comparing with the data from the literature for this histotype,[3,5,6,21-24] the abdominal lymph nodes are the most frequent metastatic site (59/87; 68%), followed by the bones (23/87; 26%), the liver (18/87; 21%), the lungs (18/87; 21%), the peritoneum (11/87; 13%), and the adrenal glands (11/87; 13%). Conversely, other more common histotypes of renal cell carcinoma, especially clear cell, much more frequently involve the lungs and the bones rather than lymph nodes (21.8%) or the peritoneum (<3%)[25] (Table 5). In this view, papillary and chromophobe renal cell carcinomas commonly display nodal metastases[26] but are more likely to involve the lungs and the liver than FH-deficient renal cell carcinomas and show less frequently a peritoneal spread (4%-5%). Similar considerations apply to other rare molecularly defined renal cell carcinoma histotypes. Although TFE3-rearranged renal cell carcinoma often behaves aggressively[27] similar to FH-deficient renal cell carcinoma, secondary localizations from this neoplasm tend to show a quite homogenous distribution among the lymph nodes (29%), the lungs (25%), the liver (17%), and the bones (13%). TFEB-rearranged renal cell carcinoma usually displays more indolent behavior, with only 12 metastatic cases reported so far, none occurring in the peritoneum,[28] and shows a hematogenous spread, with the lungs (38%), the liver (23%), and the bones (23%) more commonly involved than the lymph nodes (15%). On the other hand, TFEB-amplified renal cell carcinoma often displays a more severe clinical outcome with distant metastases being observed in almost half of the cases (44%),[29] typically with synchronous involvement of multiple organs, including the lungs (47%), the lymph nodes (47%), the liver (29%), and the bones (29%), among others. Finally, ALK-rearranged renal cell carcinoma generally localized to the regional lymph nodes (83%), without examples of peritoneal spread.[1]

In general, we can infer that FH-deficient renal cell carcinoma is much more likely to spread via the lymphatic channels and the peritoneal surface rather than directly metastasizing through hematic vessels to distant organs such as the lungs and the bones. However, these tumors tend to behave aggressively regardless of the way of metastatic spread, with comparable mean and median overall survival latency in patients with confined local/nodal localization vs systemic ones (22.5 and 31.5 vs 21.6 and 33 months, respectively). Additionally, it is worth mentioning that radiological involvement of the adrenal glands has been described in 5% to 10% of patients with hereditary leiomyomatosis and renal cell carcinoma[30,31] and reported in 13% of cases in our review. Nevertheless, at surgical resection, most of the preoperatively identified adrenal lesions were caused by macronodular hyperplasia at definitive pathologic examination.[32,33] Hence, the radiological adrenal gland involvement should raise a concern about a hyperplastic process, especially when bilateral and confined to this organ, advocating bioptic sampling if highly suspicious of a metastatic localization.

Another challenging morphologic characteristic of FH-deficient renal cell carcinoma is the occurrence of tumors with bland-looking oncocytic features. Although some of these cases showed low-grade areas admixed with more classic microscopically aggressive ones,[34] a restricted but still relevant proportion was entirely made up of cytologically eosinophilic low-grade cells with homogeneous architectural patterns. Apart from the present study, 9 cases of these pure so-called "low-grade oncocytic FH-deficient renal cell carcinomas" have been described to date, along with 3 other examples intermixed with high-grade areas.[35] Our series further widens the current knowledge on such a topic, adding another "pure" low-grade FH-deficient renal cell carcinoma to the cohort. As in similar reported cases, the tumors of our series were composed of nested to alveolar bland eosinophilic cells, resembling other low-grade oncocytic neoplasms of the kidney, including oncocytoma, hybrid oncocytic chromophobe tumor, "low-grade oncocytic tumor,"[36] "eosinophilic vacuolated renal tumor,"[37] "eosinophilic solid and cystic renal cell carcinoma,"[38] and, especially, SDH-deficient renal cell carcinoma.[39] As recently questioned,[40,41] the "pure" case described in this study behaved indolently with evidence of neither local recurrence nor distant metastases on follow-up. It is worth mentioning that the present tumor had been entirely embedded, avoiding potential biases of an unsampled "high-grade" component. So, our data further support the need to include SDH-like FH-deficient renal cell carcinomas among the potential differential diagnosis of low-grade oncocytic renal neoplasms and to perform the proper clinical and pathologic investigations.

With respect to therapy, in the current study, we have also investigated the PD-1/PD-L1 expression and *EGFR* mutations as possible predictive biomarkers. Nowadays, therapeutic strategies for patients with advanced renal cell carcinoma generally cover combinations of ICIs with various antiangiogenetic drugs.[42] However, current therapies have been mainly developed for clear cell renal cell carcinoma, and very few data are currently available regarding ICI activity in rarer histotypes.[43] Although we were not

able to find PD-1 positivity in any of the neoplasms of our cohort, neither by neoplastic cells nor by TILs, IHC-relevant PD-L1 expression by tumor cells was observed in 60% of the samples, a similar percentage (69% and 58%) previously reported in a series of 13 and 53 cases, respectively, of FH-deficient renal cell carcinoma.[11,12] To note, the following comparable results were reached using different PD-L1 clones: the previous studies employed the E1L3N PD-L1 clone (Cell Signaling), whereas we chose the SP263 assay (Ventana), which is a companion diagnostic device. It is worth mentioning that similarly to the previous papers,[11,12] in our series, PD-L1 expression was higher in neoplasms with aggressive histologic features, which was as follows: both tumors with the most significant rates of PD-L1 staining (30% in case 8 and 70% in case 11) revealed nucleolar grade G4 (second to by ISUP/WHO) and displayed areas of sarcomatoid dedifferentiation. Furthermore, even though a statistical correlation with TILs among the overall cohort could not be drawn, the highest PD-L1 values (70%) were observed in the only "inflamed" neoplasm of the series (case 11), again displaying aggressive features (G4, sarcomatoid dedifferentiation). This finding aligns with data from more common histotypes, such as clear cell renal cell carcinoma, in which a heavier peri/intratumoral infiltrate is usually accustomed to morphologically aggressive tumors (G3-G4).[44] Although further studies are needed, those data could suggest routinely testing FH-deficient renal cell carcinomas for PD-L1. Hopefully, these assays could help clinicians identify a restricted but relevant proportion of patients more likely to benefit from targeted immunotherapies. These considerations would be particularly relevant in individuals with advanced/diffusely metastatic diseases. In this setting, histologic examination of small bioptic samples is often the first and unique approach to detect potential molecular therapeutic targets. So, identifying morphologic features predictive of significant PD-L1 expression, such as sarcomatoid dedifferentiation, would carry a remarkable meaning for ultimate patient clinical management.

Finally, a limited but still relevant literature evidence, represented by a few single reports[13,45] and some wider studies,[14,46] currently supports the administration of combined EGFR (erlotinib) and VEGF (bevacizumab) inhibitors in patients affected by advanced FH-deficient renal cell carcinomas. Therefore, we analyzed the *EGFR* gene status in the tumors of our series but failed to demonstrate pathogenetic mutations in any of them. Although we only tested the neoplasms of our cohort for punctiform mutations (neither *EGFR* gene amplifications nor IHC expression), our data stand against the employment of molecular analysis for *EGFR* mutations as a predictive test to forecast therapeutic response to EGFR/VEGF inhibitors so far. Accordingly, it could be reasonably ruled out that conventional pathogenetic mutations of the *EGFR* gene are the driving molecular mechanism underlying the efficacy of such drugs in patients with FH-deficient renal cell carcinoma. A possible explanation could be that FH loss of function in neoplastic cells causes high fumarate amounts to inhibit the hypoxia-inducible factor (HIF) prolyl-hydroxilase.[47] This latter enzyme favors HIF-1α and HIF-2α degradation through the Von Hippel Lindau complex in normal oxygen levels. Thus, FH deficiency leads to accumulation of these transcriptional factors, which then promotes the transcription of both the *VEGF* and glycolytic enzyme genes.[48,49] This latter phenomenon is responsible for the so-called "Warburg" effect, referring to the increased glycolytic activity of tumor cells even in conditions of oxygen availability. Similarly, it has been demonstrated that the activation of the EGFR receptor can further increase the stability of HIF factors through the PI3K/AKT pathway regardless of cellular oxygen levels.[50] On these bases, it is tempting to speculate that EGFR and VEGF inhibitors in patients with FH-deficient renal cell carcinoma act via blockage of the aforementioned pathways, finally reducing VEGF production and glycolytic activation in tumoral cells.

In conclusion, we reported the following findings: (1) FH-deficient renal cell carcinoma is characterized by heterogeneous features even in metastatic sites themselves and between primary tumor and corresponding metastatic localizations; (2) peritoneal involvement is a more frequent event in FH-deficient renal cell carcinoma than previously described and may mimic mesothelial proliferations (both hyperplasic and neoplastic processes), so a proper IHC analysis is mandatory for this differential diagnosis; (3) we added another case of "pure" low-grade SDH-looking FH-deficient renal cell carcinoma; and (4) PD-L1, conversely to *EGFR* mutations, could be a possible predictive biomarker for the therapy of these tumors.

Author Contributions

A.C. and G.M. conceived and designed the study. S.M., L.S., L.M., M.R., G.S., P.A., and M.B. performed development of methodology and writing, review, and revision of the paper. A.C., S.M., E.B., C.V., S.P., and F.M.M. executed acquisition, analysis, and interpretation of data, and performed statistical analysis. C.V. and S.P. provided technical and material support. All authors read and approved the final paper.

Data Availability

All data generated or analyzed during this study are included in this published article.

Funding

This study was funded by "Bando di ricerca finalizzata 2021 (PC: GR-2021-12374462)."

Declaration of Competing Interest

None declared.

Ethics Approval and Consent to Participate

All procedures performed in our study involving human participants received approval (Prog. 4136CESC) and were in accordance with the ethical standards of the institutional and/or national research committee and with the declaration of Helsinki.

References

1. WHO Classification of Tumours Editorial Board. WHO Classification of Tumours. *Urinary and Male Genital Tumours*. 5th ed. IARC press; 2022.
2. Caliò A, Marletta S, Brunelli M, Martignoni G. WHO 2022 classification of kidney tumors: what is relevant? An update and future novelties for the pathologist. *Pathologica*. 2022;115(1):23–31.
3. Trpkov K, Hes O, Agaimy A, et al. Fumarate hydratase-deficient renal cell carcinoma is strongly correlated with fumarate hydratase mutation and hereditary leiomyomatosis and renal cell carcinoma syndrome. *Am J Surg Pathol*. 2016;40(7):865–875.
4. Gleeson JP, Nikolovski I, Dinatale R, et al. Comprehensive molecular characterization and response to therapy in fumarate hydratase-deficient renal cell carcinoma. *Clin Cancer Res*. 2021;27(10):2910–2919.
5. Merino MJ, Torres-Cabala C, Pinto P, Linehan WM. The morphologic spectrum of kidney tumors in hereditary leiomyomatosis and renal cell carcinoma (HLRCC) syndrome. *Am J Surg Pathol*. 2007;31(10):1578–1585.
6. Lau HD, Chan E, Fan AC, et al. A clinicopathologic and molecular analysis of fumarate hydratase-deficient renal cell carcinoma in 32 patients. *Am J Surg Pathol*. 2020;44(1):98–110.
7. Smith SC, Trpkov K, Chen YB, et al. Tubulocystic carcinoma of the kidney with poorly differentiated foci: a frequent morphologic pattern of fumarate

hydratase-deficient renal cell carcinoma. *Am J Surg Pathol*. 2016;40(11):1457–1472.
8. Muller M, Guillaud-Bataille M, Salleron J, et al. Pattern multiplicity and fumarate hydratase (FH)/S-(2-succino)-cysteine (2SC) staining but not eosinophilic nucleoli with perinucleolar halos differentiate hereditary leiomyomatosis and renal cell carcinoma-associated renal cell carcinomas from kidney tumors without FH gene alteration. *Mod Pathol*. 2018;31(6):974–983.
9. Shyu I, Mirsadraei L, Wang X, et al. Clues to recognition of fumarate hydratase-deficient renal cell carcinoma: findings from cytologic and limited biopsy samples. *Cancer Cytopathol*. 2018;126(12):992–1002.
10. Bersanelli M, Rebuzzi SE, Roviello G, Catalano M, Brunelli M, Rizzo M. Immune checkpoint inhibitors in non-conventional histologies of renal-cell carcinoma. *Hum Vaccin Immunother*. 2023;19(1):2171672.
11. Alaghehbandan R, Stehlik J, Trpkov K, et al. Programmed death-1 (PD-1) receptor/PD-1 ligand (PD-L1) expression in fumarate hydratase-deficient renal cell carcinoma. *Ann Diagn Pathol*. 2017;29:17–22.
12. Walter B, Gil S, Naizhen X, et al. Determination of the expression of PD-L1 in the morphologic spectrum of renal cell carcinoma. *J Cancer*. 2020;11(12):3596–3603.
13. Tomar S, Kashyap L, Kapoor A. Fumarate hydratase-deficient renal cell carcinoma in extended remission with bevacizumab and erlotinib. *Ecancermedicalscience*. 2022;16:1404.
14. Srinivasan R, Gurram S, Al Harthy M, et al. Results from a phase II study of bevacizumab and erlotinib in subjects with advanced hereditary leiomyomatosis and renal cell cancer (HLRCC) or sporadic papillary renal cell cancer. *J Clin Oncol*. 2020;38:5004.
15. Smith SC, Sirohi D, Ohe C, et al. A distinctive, low-grade oncocytic fumarate hydratase-deficient renal cell carcinoma, morphologically reminiscent of succinate dehydrogenase-deficient renal cell carcinoma. *Histopathology*. 2017;71(1):42–52.
16. Binnewies M, Roberts EW, Kersten K, et al. Understanding the tumor immune microenvironment (TIME) for effective therapy. *Nat Med*. 2018;24(5):541–550.
17. Takahara T, Murase Y, Tsuzuki T. Urothelial carcinoma: variant histology, molecular subtyping, and immunophenotyping significant for treatment outcomes. *Pathology*. 2021;53(1):56–66.
18. Al-Hussain TO, Cheng L, Zhang S, Epstein JI. Tubulocystic carcinoma of the kidney with poorly differentiated foci: a series of 3 cases with fluorescence in situ hybridization analysis. *Hum Pathol*. 2013;44(7):1406–1411.
19. Chand MT, Edens J, Lin T, Anderson I, Berri R. Benign multicystic peritoneal mesothelioma: literature review and update. *Autops Case Rep*. 2020;10(3):e2020159.
20. Kusamura S, Baratti D, De Simone M, et al. Diagnostic and therapeutic pathway in diffuse malignant peritoneal mesothelioma. *Cancers (Basel)*. 2023;15(3):662.
21. Chen Y-B, Brannon AR, Toubaji A, et al. Hereditary leiomyomatosis and renal cell carcinoma syndrome-associated renal cancer: recognition of the syndrome by pathologic features and the utility of detecting aberrant succination by immunohistochemistry. *Am J Surg Pathol*. 2014;38(5):627–637.
22. Kuroda N, Tsutsui M, Iguchi M, et al. Fumarate hydratase-deficient renal cell carcinoma: a clinicopathological study of seven cases including hereditary and sporadic forms. *Ann Diagn Pathol*. 2020;49:151599.
23. Udager AM, Alva A, Chen Y-B, et al. Hereditary leiomyomatosis and renal cell carcinoma (HLRCC): a rapid autopsy report of metastatic renal cell carcinoma. *Am J Surg Pathol*. 2014;38(4):567–577.
24. Liang J, Sun G, Pan X, et al. Genomic and transcriptomic features between primary and paired metastatic fumarate hydratase-deficient renal cell carcinoma. *Genome Med*. 2023;15(1):31.
25. Bianchi M, Sun M, Jeldres C, et al. Distribution of metastatic sites in renal cell carcinoma: a population-based analysis. *Ann Oncol*. 2012;23(4):973–980.
26. Dudani S, de Velasco G, Wells JC, et al. Evaluation of clear cell, papillary, and chromophobe renal cell carcinoma metastasis sites and association with survival. *JAMA Netw Open*. 2021;4(1):e2021869.
27. Caliò A, Segala D, Munari E, Brunelli M, Martignoni G. MiT family translocation renal cell carcinoma: from the early descriptions to the current knowledge. *Cancers (Basel)*. 2019;11(8):1110.
28. Caliò A, Brunelli M, Segala D, et al. t(6;11) renal cell carcinoma: a study of seven cases including two with aggressive behavior, and utility of CD68 (PG-M1) in the differential diagnosis with pure epithelioid PEComa/epithelioid angiomyolipoma. *Mod Pathol*. 2018;31(3):474–487.
29. Kammerer-Jacquet S-F, Gandon C, Dugay F, et al. Comprehensive study of nine novel cases of TFEB-amplified renal cell carcinoma: an aggressive tumour with frequent PDL1 expression. *Histopathology*. 2022;81(2):228–238. https://doi.org/10.1111/his.14683
30. Smit DL, Mensenkamp AR, Badeloe S, et al. Hereditary leiomyomatosis and renal cell cancer in families referred for fumarate hydratase germline mutation analysis. *Clin Genet*. 2011;79(1):49–59.
31. Matyakhina L, Freedman RJ, Bourdeau I, et al. Hereditary leiomyomatosis associated with bilateral, massive, macronodular adrenocortical disease and atypical Cushing syndrome: a clinical and molecular genetic investigation. *J Clin Endocrinol Metab*. 2005;90(6):3773–3779.
32. Arora R, Eble JN, Pierce HH, et al. Bilateral ovarian steroid cell tumours and massive macronodular adrenocortical disease in a patient with hereditary leiomyomatosis and renal cell cancer syndrome. *Pathology*. 2012;44(4):360–363.
33. Shuch B, Ricketts CJ, Vocke CD, et al. Adrenal nodular hyperplasia in hereditary leiomyomatosis and renal cell cancer. *J Urol*. 2013;189(2):430–435.
34. Hamza A, Sirohi D, Smith SC, Amin MB. Low-grade oncocytic fumarate hydratase-deficient renal cell carcinoma: an update on biologic potential, morphologic spectrum, and differential diagnosis with other low-grade oncocytic tumors. *Adv Anat Pathol*. 2021;28(6):396–407.
35. Wyvekens N, Anderson WJ, Kim YX, Carter M, Hirsch MS. Low-grade fumarate hydratase-deficient renal cell carcinoma in a 30-year-old female. *Int J Surg Pathol*. 2022;30(2):184–189.
36. Trpkov K, Williamson SR, Gao Y, et al. Low-grade oncocytic tumour of kidney (CD117-negative, cytokeratin 7-positive): a distinct entity? *Histopathology*. 2019;75(2):174–184.
37. Tjota M, Chen H, Parilla M, Wanjari P, Segal J, Antic T. Eosinophilic renal cell tumors with a TSC and MTOR gene mutations are morphologically and immunohistochemically heterogenous: clinicopathologic and molecular study. *Am J Surg Pathol*. 2020;44(7):943–954.
38. Trpkov K, Hes O, Bonert M, et al. Eosinophilic, solid, and cystic renal cell carcinoma: clinicopathologic study of 16 unique, sporadic neoplasms occurring in women. *Am J Surg Pathol*. 2016;40(1):60–71.
39. Gill AJ, Pachter NS, Chou A, et al. Renal tumors associated with germline SDHB mutation show distinctive morphology. *Am J Surg Pathol*. 2011;35(10):1578–1585.
40. Smith SC, Hamza A, Sirohi D, Amin MB. Response to the letter to the editor entitled "Do we have sufficient evidence to define prognosis for 'low-grade' fumarate hydratase-deficient renal cell carcinoma?". *Adv Anat Pathol*. 2022;29(3):181–182.
41. Gupta S, Menon S, Raghunathan A, Herrera-Hernandez L, Jimenez RE, Cheville JC. Do we have sufficient evidence to define prognosis for "low-grade" fumarate hydratase-deficient renal cell carcinoma? *Adv Anat Pathol*. 2022;29(3):178–181. https://doi.org/10.1097/PAP.0000000000000335
42. Motzer R, Alekseev B, Rha S-Y, et al. Lenvatinib plus pembrolizumab or everolimus for advanced renal cell carcinoma. *N Engl J Med*. 2021;384(14):1289–1300.
43. Choueiri TK, Fay AP, Gray KP, et al. PD-L1 expression in nonclear-cell renal cell carcinoma. *Ann Oncol*. 2014;25(11):2178–2184.
44. Marletta S, Caliò A, Bogina G, et al. STING is a prognostic factor related to tumor necrosis, sarcomatoid dedifferentiation, and distant metastasis in clear cell renal cell carcinoma. *Virchows Arch*. 2023;483(1):87–96.
45. Park I, Shim YS, Go H, Hong BS, Lee JL. Long-term response of metastatic hereditary leiomyomatosis and renal cell carcinoma syndrome associated renal cell carcinoma to bevacizumab plus erlotinib after temsirolimus and axitinib treatment failures. *BMC Urol*. 2019;19(1):51.
46. Choi Y, Keam B, Kim M, et al. Bevacizumab plus erlotinib combination therapy for advanced hereditary leiomyomatosis and renal cell carcinoma-associated renal cell carcinoma: a multicenter retrospective analysis in Korean patients. *Cancer Res Treat*. 2019;51(4):1549–1556.
47. Baksh SC, Finley LWS. Metabolic coordination of cell fate by α-ketoglutarate-dependent dioxygenases. *Trends Cell Biol*. 2021;31(1):24–36.
48. Peng X-H, Karna P, Cao Z, Jiang B-H, Zhou M, Yang L. Cross-talk between epidermal growth factor receptor and hypoxia-inducible factor-1alpha signal pathways increases resistance to apoptosis by up-regulating survivin gene expression. *J Biol Chem*. 2006;281(36):25903–25914.
49. Linehan WM, Rouault TA. Molecular pathways: fumarate hydratase-deficient kidney cancer–targeting the Warburg effect in cancer. *Clin Cancer Res*. 2013;19(13):3345–3352.
50. Naumov GN, Nilsson MB, Cascone T, et al. Combined vascular endothelial growth factor receptor and epidermal growth factor receptor (EGFR) blockade inhibits tumor growth in xenograft models of EGFR inhibitor resistance. *Clin Cancer Res*. 2009;15(10):3484–3494.